Grading version.

MSc Physics report University of Groningen*

Single-particle visualization of chikungunya and dengue viruses

Jelle S. Blijleven

25th August 2013

*Under supervision of Antoine M. van Oijen, Single-molecule Biophysics.

Chikungunya and dengue are tropical viruses for which no vaccine is available. The research presented shows the design challenges associated with observing single-particle hemifusion kinetics of these viruses, in the long term useful for e.g. antiviral drug screening.

The timescale of chikungunya fusion was determined to be in the order of a second, which is at the edge of the detection limit for the current setup. The main challenges were keeping a constant, high temperature and ensuring the acidification to be synchronized and short. A new flow channel design was made countering the challenges. Preliminary data indicated dengue fusion to take about 15 seconds.

A theoretical excercise showed that the channel aspect ratio optimized for the highest average velocity at the edge of the channel is $r \approx 1.3$. Finally, the foundation was laid of a new software package to do automated viral fusion analysis.

A single-particle study as begun in this report of chikungunya is therefore both pioneering and a promising road towards antiboy screening.

Contents

1 Viral fusion

Once a virus has entered the human body, its work is far from done. It has to enter a cell bypassing the cell digestive system to have its genome delivered intact, whereafter the viral genome can take control and reproduction can begin. Viruses like influenza cleverly make use of the cell digestive route to accomplish this and fuse their own envelope with that of the host cell. This report is concerned mainly with the design of an experimental setup in which we can observe such viral fusion events at the single-particle level. It will be utilized to to infer fundamental the biochemical processes and intermediates in the process of viral entry. Ultimately, such an assay could be used to screen antiviral drugs.

The virses under study use a similar mechanism of entry to influenza.

1.1 The viruses: chikungunya and dengue

Although mostly considered not to be a life-threatening disease, recent outbreaks in the Western world and the first documented deaths in 2006 have attracted the attention of researchers towards chikungunya virus (chikv). Its geographical domain lies throughout large tropical regions in Africa and India (figure 1.1). It is an arbovirus, spread by arthropods (mosquitos), between humans and from monkey populations acting as reservoirs of potential new outbreaks. Typical symptoms after infection are a high fever lastings several days, skin rashes, headaches and arthralgia. The latter, joint pains, can be very incapacitating, and last and relapse for several months. This may have lead to the virus name which would mean 'bent up' in a local African language. Chikungunya is a relatively unknown and poorly studied virus and hence no vaccine or treatment is available so far [Pialoux et al., 2007].

Dengue is also a tropical virus similarly spread via mosquitos over larger portions of the world and for which no vaccine is available. Both viruses are expected to enlarge their distributions due to global warming.

As all viruses studied in the assay that will be presented in this report, chikungunya (alphavirus family) and dengue (flavivirus) have a phospholipid envelope which has to merge, or fuse, with the membrane of the target cell [Martín et al., 2009]. They have a capsid containing positive-sense single-stranded RNA (see figure 1.3a for dengue, and a different alphavirus, Semliki-forest virus). As depicted, the outside of the virus is densely packed with transmembrane glycoproteins: the fusion machinery. Chikungunya is typically 70 nm in diameter, against 55 nm for dengue. This is clearly much smaller than the eye can see and also smaller than the wavelength of visible light.

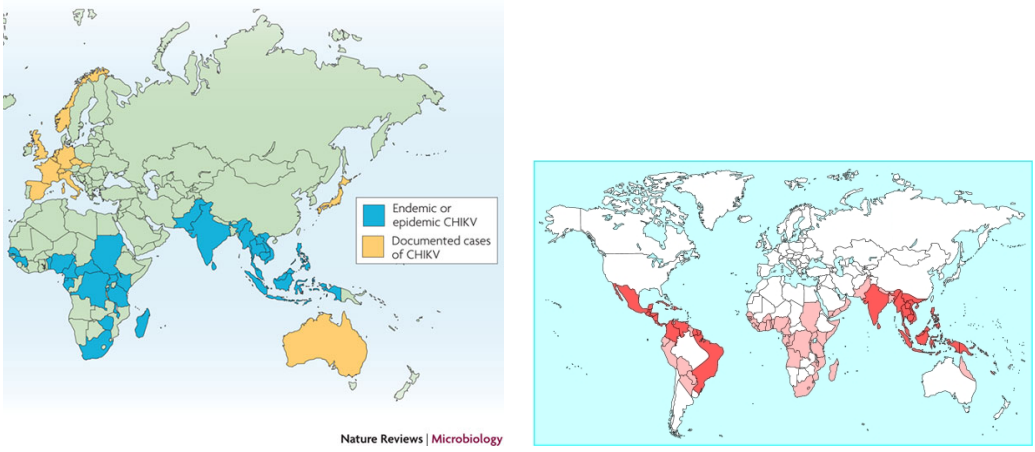

Figure 1.1: Left: chikungunya geographical distribution. Figure from [Schwartz and Albert, 2010]. Right: dengue geographical distribution. Figure from [Gibbons and Vaughn, 2002].

1.2 Pathway of entry and fusion mechanism

In figure 1.2 the general alphavirus infection pathway is depicted. The virion attaches to target cell receptors and is taken up by endocytosis, after which the virus particle resides in an endosome within the target cell. During endosomal maturation the internal acidity lowers to pH 5, usually leading to the digestion of the endosomal contents. However, the low pH is also the trigger that makes the virus particle fuse with the endosome membrane, allowing the viral genome to enter the cell [Kielian and Rey, 2006].

The acidification of the aqueous environments of the virus particle leads to protonation of the transmembrane glycoproteins in the envelope of the virus, which then trigger membrane fusion. For alphaviruses and flaviviruses, there are two proteins: one that can do work towards membrane fusion and a companion protein; these are designated E1 and E2 respectively for alphaviruses and E and M for flaviviruses. Figures 1.3a and 1.3c show that the E1 fusion protein and E2 companion protein form a tightly fitting heterodimer organized in a trimeric fashion on the alphavirus surface. E2 protects the E1 fusion peptide which is part of an internal loop. In flaviviruses, the E transmembrane protein is both the fusion protein and the receptor binding protein. It forms a homodimer on the dengue surface, in which the fusion peptide is shielded inbetween the two E units. An important step in the maturation of dengue virus is shown in figure 1.3b: during virion formation the E protein is cotranslationally folded with a prM protein and the virus is not fusogenic until the prM has been cleaved to M.

Upon protonation the viral transmembrane proteins undergo several conformational changes, figure 1.3c. In alphaviruses, the E2 companion protein moves out of the way. The E1 then forms an extended intermediate state inserting the fusion peptide loop into the target membrane, after which the fusion proteins organise into homotrimers (b–

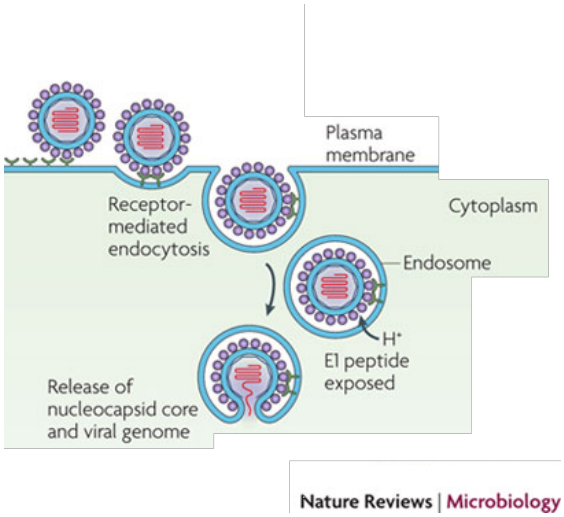

Figure 1.2: The alphavirus infection pathway. This report focuses on the fusion of the virion with the endosome. Figure adapted from [Schwartz and Albert, 2010]

c). In flaviviruses the E-E homodimers dissociate after which they also homotrimerize. The E or E1 trimers then cooperatively undergo a jackknife-like conformational change, bringing the virus and target membrane to hemifusion, a state in which the proximal leaflets are fused and lipids can freely mix. Finally the full fusion pore is formed allowing content mixing (d–f).

There are several reasons for which it can be very fruitful to turn to single-particle studies of Chikungunya virus. Until now, alphavirus data was mostly obtained from Semliki-Forest virus. Semliki Forest virus fusion is known to be cholesterol and sphingolipid dependent [Kielian and Rey, 2006], and a bulk study has confirmed this for chikungunya as well (M.K.S. Richter, unpublished). There are indications from crystallization data of the alphavirus fusion protein that rings of 5 or 6 homotrimers of E1 act cooperatively in establishing the membrane fusion [Kielian and Rey, 2006]. Lastly, for influenza virus, a single-molecule study has shown the amount of antibodies bound that is necessary to neutralize the virion fusogenicity and porting this to chikungunya and dengue might help towards vaccine development.

The next chapter introduces the methods.

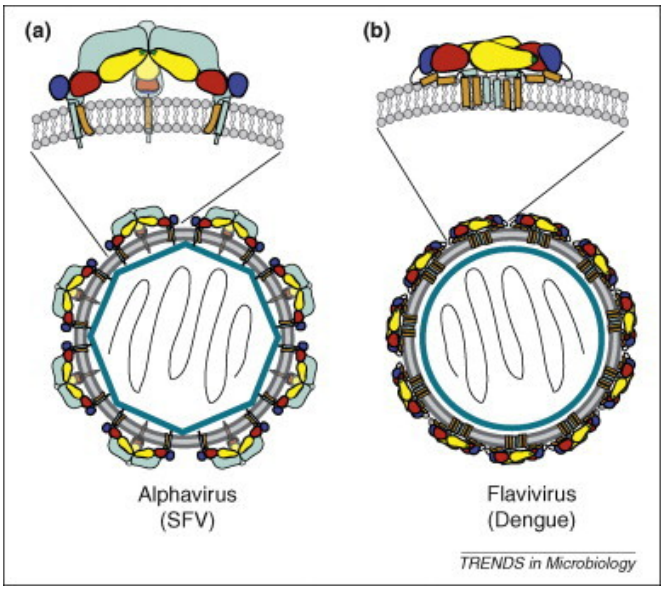

(a) Virus layout. Shown are the virion lipid bilayer membrane in which the fusion protein is anchored and the capsids containg the viral genome. a. An alphavirus. b. Dengue.

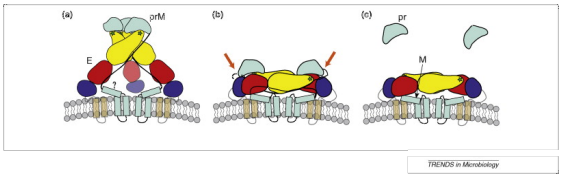

(b) Flavivirus prM companion cleavage shown in a.–c. is the maturation step of dengue essential for fusogenicity.

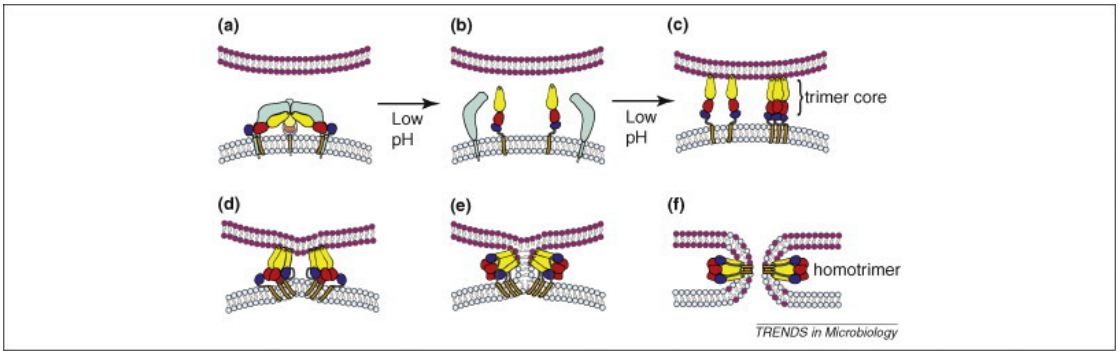

(c) Alphavirus fusion mechanism intermediate steps. a.–b. show the freeing and extension of the fusion proteins c. extended intermediate homotrimers e. hemifusion f. pore formation.

Figure 1.3: Alphavirus and flavivirus layout and fusion proteins. In yellow the fusion protein, the companion protein in cyan. Images from [Martín et al., 2009].

2 The viral fusion assay

2.1 Virus docking

Observation of viral hemifusion and fusion pore formation events on a single-particle level with a controlled pH drop was demonstrated by Floyd et al. [2008]. Information was obtained about intermediate states in the process of viral membrane fusion. The text below will briefly introduce their method as implemented in this research.

To make an environment in which the virus particle hemifusion can be observed, a lipid bilayer is created on a glass coverslip. The lipids are added to a microfluidic channel formed by PDMS in the form of liposomes of nominally 100 μm diameter, at a concentration of 2 mM in HNE buffer (5 mM hepes, 150 mM NaCl, 0.1 mM EDTA, pH adjusted to 7.4). The liposomes then are incubated for at least 20 minutes to form a lipid bilayer naturally through interactions of the lipid head groups with the hydrophylic glass surface.

Incorporated into the bilayer is biotinylated phosphatidylethanolamine (B-PE) to which streptavidin-fluorescein can bind. It is flown in and with high affinity ($K_d \simeq 10^{-2}$ pM) binds to the B-PE. Washing with HNE buffer removes superfluous fluorescein in solution. The fluorescein equilibrium between the dianion and monoanion state as in figure 2.1 has a p$K_a \simeq 6.4$, with the monoanion having significantly lower fluorescence [Sjöback et al., 1995], leading to a drastic decrease in fluorescence at pH ≤ 6. The drop in fluorescein fluorescence can be used to determine the 't equals zero' of the experiment.

The virus is flown in at a concentration of typically mM and incubated until a density of about 300 particles in the field of view is attained.

To start the experiment, the environment of the virus is acidified by flowing in low pH buffer with sufficient speed, synchronizing the fusion events of each virion.

2.2 Fluorescence total internal reflection microscopy

The viral membrane is labelled with the lipophylic dye octadecyl rhodamine B (R18), see figure 2.2, which self-quenches at high concentrations. To be able to discern such small particle single-particle fluorescence care must be taken to minimize background fluorescence, as described below.

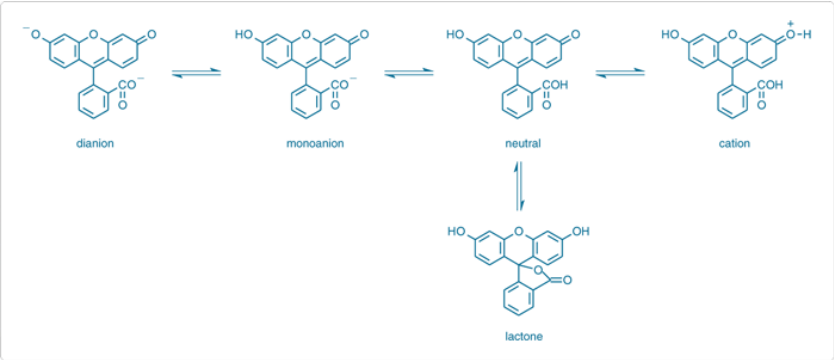

Figure 2.1: Ionization equilibria of fluorescein. From left to right, upper row: $pK_1 = 6.43$, $pK_2 = 4.31$, and $pK_3 = 2.08$ [Sjöback et al., 1995].

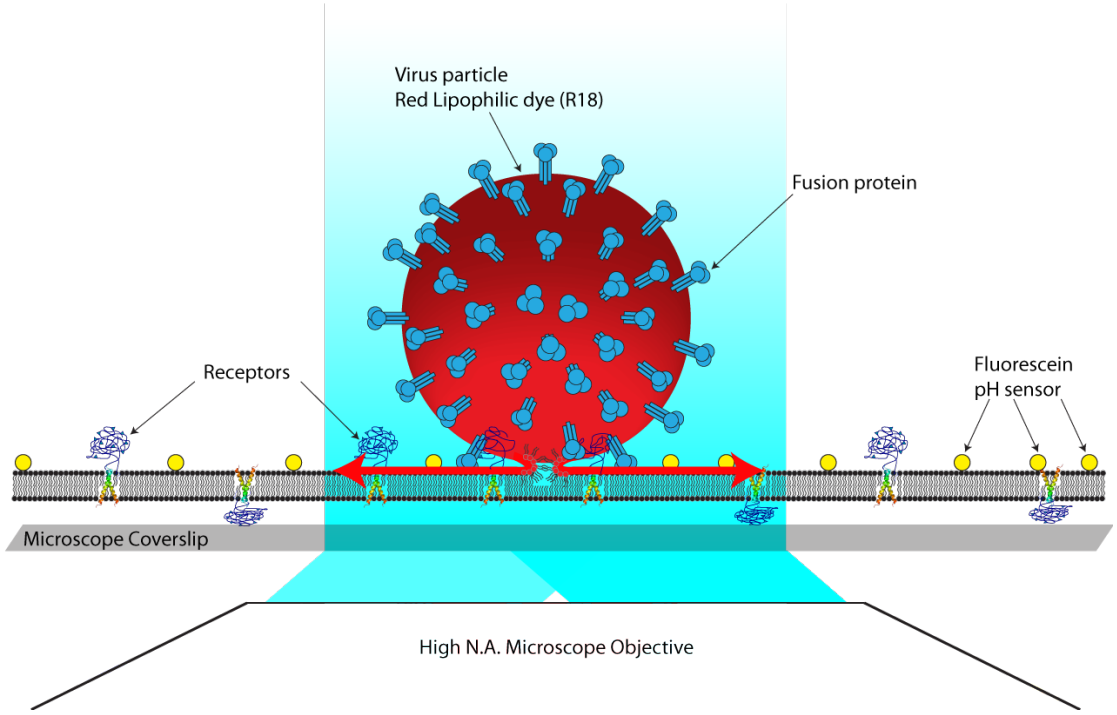

Figure 2.2: Virus docked onto glass supported lipid bilayer. Image adapted from J. Otterstrom.

The setup is equipped with two excitation lasers at 488 nm and 561 nm. These are tailored to be near the absorption maxima of fluorescein, the pH sensor dye, and R18, the lipophylic membrane labelling dye.

The longer wavelength laser is guided through a dichroic mirror to coincide with the reflected lower wavelength laser light. Then they are both reflected upwards into the microscope with a band-pass dichroic mirror. The laser beams are guided and focused with an angle of incidence onto the glass coverslip to achieve *total internal reflection microscopy* (TIRFM). The evanescent wave from the total internal reflection only excites a region up to ~ 100 nm behind the coverslip, hence limiting the background fluorescence. The resulting fluorescence of the fluorescein and R18 dyes is collected via the reflecting band-pass dichroic into a DualView2 unit, which splits the beam to enable simultaneous imaging of the two dyes' fluorescences onto different halves of an EM-CCD camera, see figure 2.4. Optionally, to do experiments at 37 °C the flow cell is heated by a heating insert in conjuction with an objective heater.

Upon hemifusion of the proximal leaflets of the lipid bilayers of the virus and the target membrane, the membrane dye can escape, yielding an intensity increase from the dequenching and then decrease from the dissipation of the dye (see figure .2.3). The intensity in time from the diffraction-limited spots can be extracted to yield exact timing information of the acidification, via the green channel fluorescein fluorescence, and of the hemifusion dequenching signal in the red channel.

2.3 Data analysis

Figure 2.5 shows the steps necessary to extract the data from the movie files. The steps are:

1. Background correction and illumination correction for Gaussian beam profile.
2. Determination of the pH drop from the green emission channel.
3. Particle detection in the red emission channel using discoidal filtering.
4. For every particle, extract the integrated intensity over the course of a recorded fusion movie.
5. Selection of the particles that show a hemifusion event is done manually by visual inspection of the fluorescence intensities over time for all detected particles.

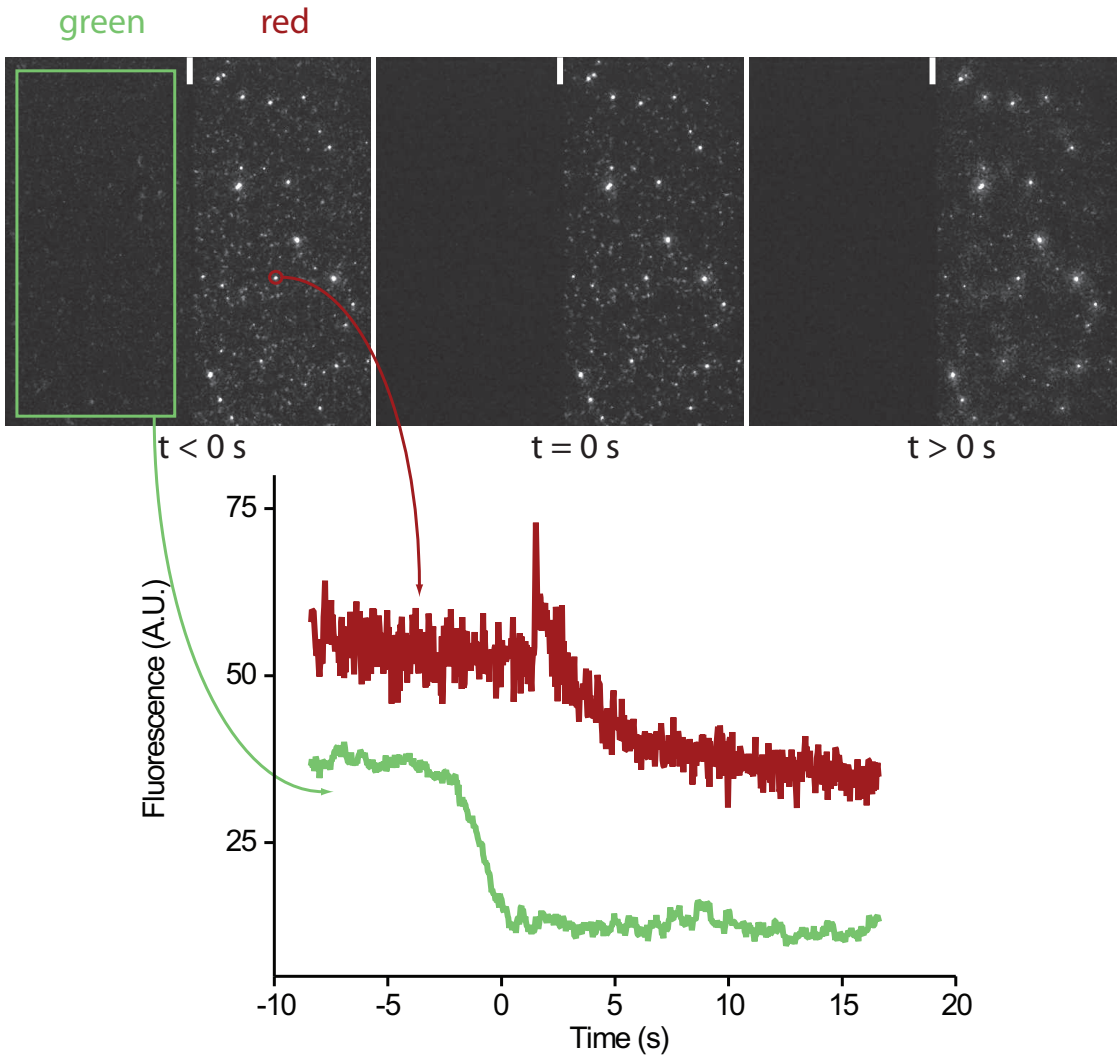

Figure 2.3: Intensity extraction. Top row shows movie frames of the two fluorescence color channels as collected onto two different halves of an EM-CCD camera. The fluorescence intensity of the fluorescein pH signal (green) and the R18 membrane dye (red) provide exact timing of single-particle hemifusion events. Scale bar (white inset in movie frames) 10 μm.

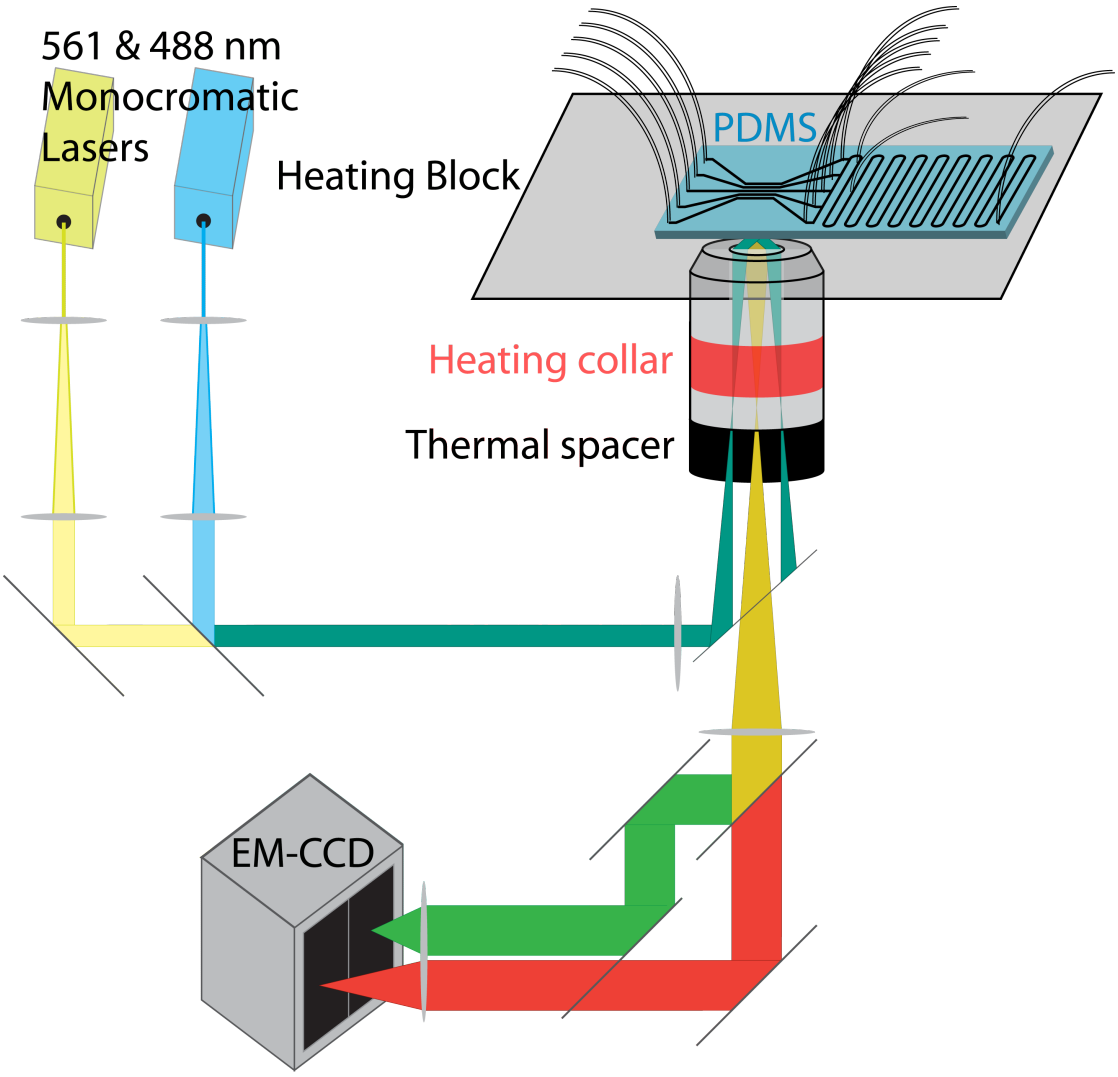

Figure 2.4: Setup as used to excite and collect dye fluoresence from the flow cell onto two halves of the camera. The 488 nm and 561 nm excitation lasers are combined and excite the sample by the evanescent wave from TIRF. The resulting fluorescence is split into two color channels, each projected on a half of the EM-CCD camera to allow for simultaneous imaging of the pH drop and hemifusion events. The flow cell and objective are kept at high temperature. Image adapted from J. Otterstrom.

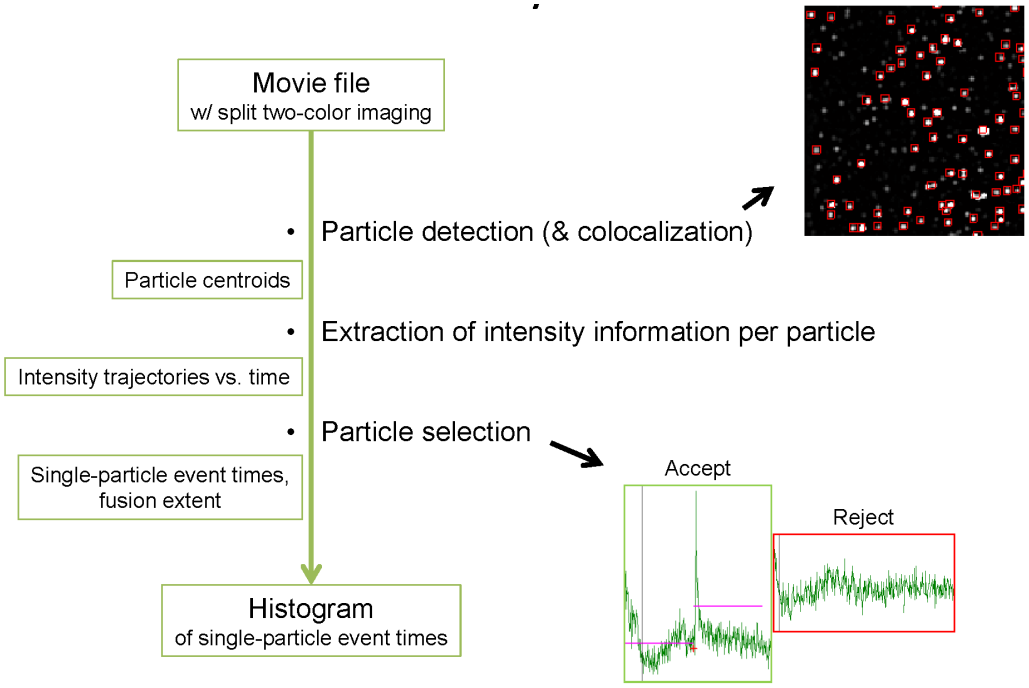

Figure 2.5: Viral fusion data flow.

3 Microfluidic flow in a rectangular channel

The chikungunya hemifusion time was determined to be around 1 s (see next chapter) which is shorter than the typical acidification time of 4–6 s the current setup could provide. Since changing the channel aspect ratio changes the form of the flow profile in the channel, as demonstrated below, it is worthwhile to check theoretically if we can optimize the channel geometry to give the fastest acidification time.

Since we are looking at single particles packed in an area of only 140 μm by 70 μm, the flow cell is of comparable width and height. The volumes of virus and liposome suspension and the different buffers can thus be kept small, on the order of microliters, and the buffer environment of the virus particles can be quickly exchanged to lower the pH. At such small scales fluid flows behave differently than what we are used to in daily life — what *small* means and relative to what it is small will become clear shortly. The following text derives mostly from [Stone, 2007, Squires and Quake, 2005, Purcell, 1976].

3.1 Dimensional considerations

Whenever fluid in a channel is subjected to a pressure difference along the length of that channel it will experience a net force and therefore start to flow. The viscosity of the fluid, that is, it's tendency to propagate momentum gradients, and the 'no-slip' boundary conditions (the velocity of the fluid at the walls should be equal to that of the walls, i.e. zero) make that the fluid experiences a viscous drag force resisting the flow. The hydrodynamic pressure gradient along the channel has both to overcome this friction in the form of the viscosity of the fluid, and to accelerate the fluid to overcome inertia. The dimensionless number expressing the relative magnitudes of these two responses is the *Reynolds number* $\mathcal{R}$, equation 3.1. The number can by dimensional analysis be obtained from considering the relevant physical quantities for fluid flow[Goldreich et al., 1999]:

$$\frac{\text{mass} \cdot \text{acceleration}}{\text{viscous forces}} \sim \frac{\rho l^3 \cdot \mu/(l/v)}{\mu v/l^2} = vl\frac{\rho}{\mu} = \frac{vl}{\nu} \equiv \mathcal{R} \tag{3.1}$$

With ρ, μ and ν the density, shear viscosity and dynamic viscosity of the fluid respectively, v the fluid speed and l the typical length scale of the channel involved.

Therefore, to make a distinction between flow speed regimes, we can use the dimensionless Reynolds number: it depends purely on the properties of the fluid and the particular geometry involved. In general, fluid flows with $\mathcal{R} \gtrsim 2000$ will behave *turbulently*: the

inertial forces dominate and the fluid will show eddies and mixing, whereas for lower Reynolds numbers the flow is *laminar* and there is almost no mixing between adjacent layers of the fluid: the fluid propagates in a laminar fashion. For very low Reynolds numbers, $\mathcal{R} \ll 1$, the viscous forces dominate completely leading to *Stokes flow* or *creeping flow*.

In this case the microfluidic channel has a $0.1\,\mathrm{mm}^2$ cross-section, low pH buffer flow rate of typically $200\,\mu\mathrm{L\,min}^{-1}$ and (water) shear viscosity and density of $10^{-3}\,\mathrm{kg\,m}^{-1}\mathrm{s}^{-1}$ and $10^3\,\mathrm{kg\,m}^{-3}$ respectively. This gives $\mathcal{R} \approx 3$, so the flow is typically very laminar and does not mix. Or the other way around, to achieve turbulent flow regimes we would need $u \approx 10\,\mathrm{m\,s}^{-1} \approx 60\,\mathrm{mL\,min}^{-1}$.

3.2 Two dimensional flow profile: optimization of pH drop time

Now consider a rectangular channel as in figure 3.1a.

In the case of a rectangular channel with height much smaller than the width $h \ll w$, the speed profile across the channel is approximately parabolic [Stone, 2007]:

$$u(y) = \frac{\Delta p}{2\mu L}\left((h/2)^2 - y^2\right) \tag{3.2}$$

The above formula is integrated to approximate the flow rate Q in the channel as:

$$Q = w\int_0^h u(y)\,dy = \frac{\Delta p}{12\mu L} w h^3 \tag{3.3}$$

For a given pressure gradient and channel width, we see that changing the height with a factor of 2 decreases the flow rate with a factor of 8. As the channel becomes smaller the hydrodynamic resistance increases with the cube and we need to increase the pressure more than we reduce the size to maintain the same flow rate.

The general axial flow speed can be given analytically in an infinite Fourier series to yield the full speed profile $u(x, y)$ and volume flow rate Q that can be approximated numerically (equation 3.4) [Schön and Weidner, 2006].

$$u(x,y) = \frac{\Delta p}{2\mu L}\left((h/2)^2 - y^2 - \sum_{n=0}^{\infty} a_n \cos(\frac{\lambda_n y}{h/2})\cosh(\frac{\lambda_n x}{h/2})\right) \tag{3.4}$$

$$Q = \frac{\Delta p}{12\mu L} w h^3 \left(1 - 6\frac{h}{w}\sum_{n=0}^{\infty} \lambda_n^{-5}\tanh(\frac{\lambda_n w}{h})\right) \tag{3.5}$$

with

$$\lambda_n = \pi(2n+1)/2$$

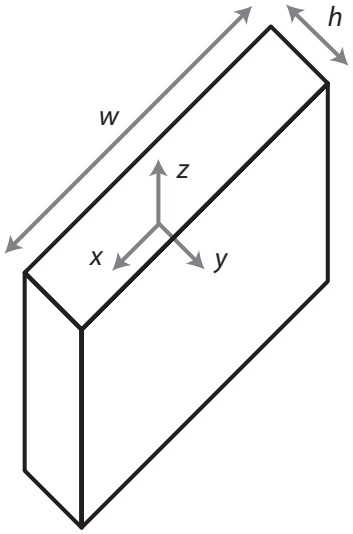

(a) Rectangular channel orientations. Fluid flow in the z-direction, particles located at either edge of the x direction, microscope objective looking along y direction.

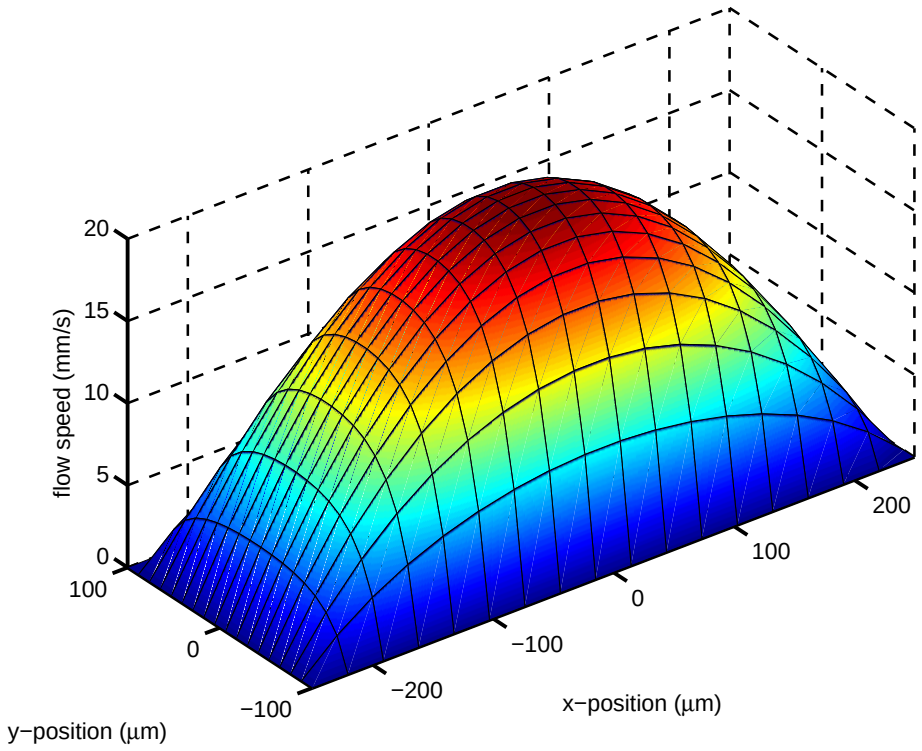

(b) Rectangular channel flow profile. 3D plot of flow speed profile in channel of dimensions $0.5\,\mathrm{mm} \times 0.2\,\mathrm{mm}$ for volume flow rate $60\,\mu\mathrm{L\,min}^{-1}$. It shows the approximately parabolic profile along the shortest dimension and a flattened parabola along the other.

Figure 3.1: Flow speed profile in the flow channel as utilized.

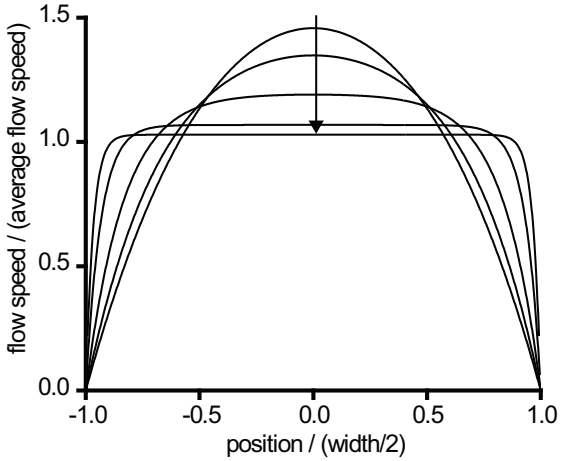

Figure 3.2: Flow speed in a cross-section of a rectangular channel for several channel dimensions. Following the arrow the channel dimensions width / height are 1, 2, 4, 10 and 20. Flow speed normalized to the average flow speed (kept constant). Position normalized to the channel width.

$$a_n = \frac{(-1)^n h^2}{\cosh(\lambda_n w/h)}$$

In figure 3.1b we see the flow profile in our channel resulting from a pumping speed of $60\,\mu\mathrm{L\,min}^{-1}$. In figure 3.2 we see the numerical values of equations 3.4 for different rectangular channel dimensions. We see that the parabolic flow profile of the square channel flattens more and more as the channel becomes flatter in the height dimension: a larger part of the channel comes closer to the average flow speed. This is reasonable since the no-slip boundary condition on the edge has less and less influence in the middle of the channel as the channel width increases.

A question arises naturally: for a given channel cross-section and pumping rate, can we increase the flow speed component close to the bottom of our channel (where the viruses are located) by choosing a different channel aspect ratio? This would lead to a shorter pH drop time if the time between starting the pH drop and its arrival were shorter than the time for the pH to diffuse all over de width of the channel. The time for the pH drop to arrive is typically 4 s in the new design. The proton diffusion coefficient is extremely high due to 'hand-over' and hopping mechanisms [Agmon, 1995] with a value of $D = 7 \cdot 10^3\,\mu\mathrm{m}^2\,\mathrm{s}^{-1}$. For two-dimensional diffusion during four seconds, the mean square diffusion distance of the protons is $\sqrt{< d^2 >} = \sqrt{4\tau D} \approx 4 \cdot 10^2\,\mu$m, or, across the whole channel. Concluding, the two timescales are similar in size, so there might be a small gain by changing the flow profile.

In the middle of the channel we can see clearly that the highest flow speed is attained with parabolic flow with about $v_{max} \approx 1.5\bar{v}$. For increasing flatness of the channel, this maximum goes down. At the edge, though, it is not clear in one glance what is

ocurring: the flow profile decreases more steeply at the edges as the channel flattens, but at the same time the width of the channel increases with increasing flatness which might dominate the previous effect for specific ratios. The effect is clarified in the to-scale channel examples of figure 3.3. Again, we see an almost parabolic profile for a square channel and for the shortest dimension in flattened channels.

The flow speed at a fixed position from the edge as a function of the channel aspect ratio is plotted in figure 3.4. This flow speed was averaged over the whole observation width as indicated in figure 3.3. The average velocity is kept constant for all different ratios by keeping the channel cross-section constant to $0.1\,\mathrm{mm}^2$ and the volume flow rate constant at $60\,\mu\mathrm{L}\cdot\mathrm{min}^{-1}$. It turns out that the optimal aspect ratio of the channel when observing from below in the height direction is $r \approx 1.3$, or a channel of $0.36\,\mathrm{mm} \times 0.28\,\mathrm{mm}$. With our channel ratio of 5:2 we are at 88 % of the optimal speed, indicated with the vertical line in the figure.

In the end, it turns out there is not much to be gained by changing the channel dimensions, but such an outcome was not clear *a priori*. With the diffusion time comparable to the arrival time of the low pH, and the design so close to optimal, there is probably no observable gain in changing the flow channel ratio to 1.3.

Furthermore, what keeps the pH drop time for pH 7.4 to pH 6 limited at about 1 s? Do the protons need a long time to diffuse close to the glass? It is known that confinement of Brownian motion reduces the effective diffusion coefficient at distances in the order of the radius of the diffusing particle [Faucheux and Libchaber, 1994], but this would not play a large role for the angstrom sized protons. Hence we hypothesize that the reaction rate for the conversion of fluorescein from a fluorescing to non-fluorescent molecule is the limiting factor since the pH used to induce fusion is close to its $p\mathrm{K_a}$ of 6.4. Consistently, lower pH experiments show a shorter pH drop time. As such, it may be necessary to find a pH-dependent dye molecule with a higher and more appropriate $p\mathrm{K}_a$value to monitor the local pH surrounding the virus particles.

As a final remark, the force acted on the chikungunya virions from the water flow is purely Stokes drag force because of the very low Reynolds number at the edge of the channel, where the flow is tending to zero. Using the Stokes drag force equation 3.6, with the dynamic viscosity of water $\mu = 10^{-3}\,\mathrm{Pa}\cdot\mathrm{s}$, particle radius $R = 35\,\mu\mathrm{m}$, and mean flow speed over the 70 nm at the edge $v = 0.0679\,\mathrm{mm}\cdot\mathrm{s}^{-1}$ from a pumping rate of $300\,\mu\mathrm{L}\cdot\mathrm{min}^{-1}$, we find an approximate force of 50 pN acting on particles in the middle of the channel during high-flow acidification.

$$F_{drag,Stokes} = 6\pi\mu R v \tag{3.6}$$

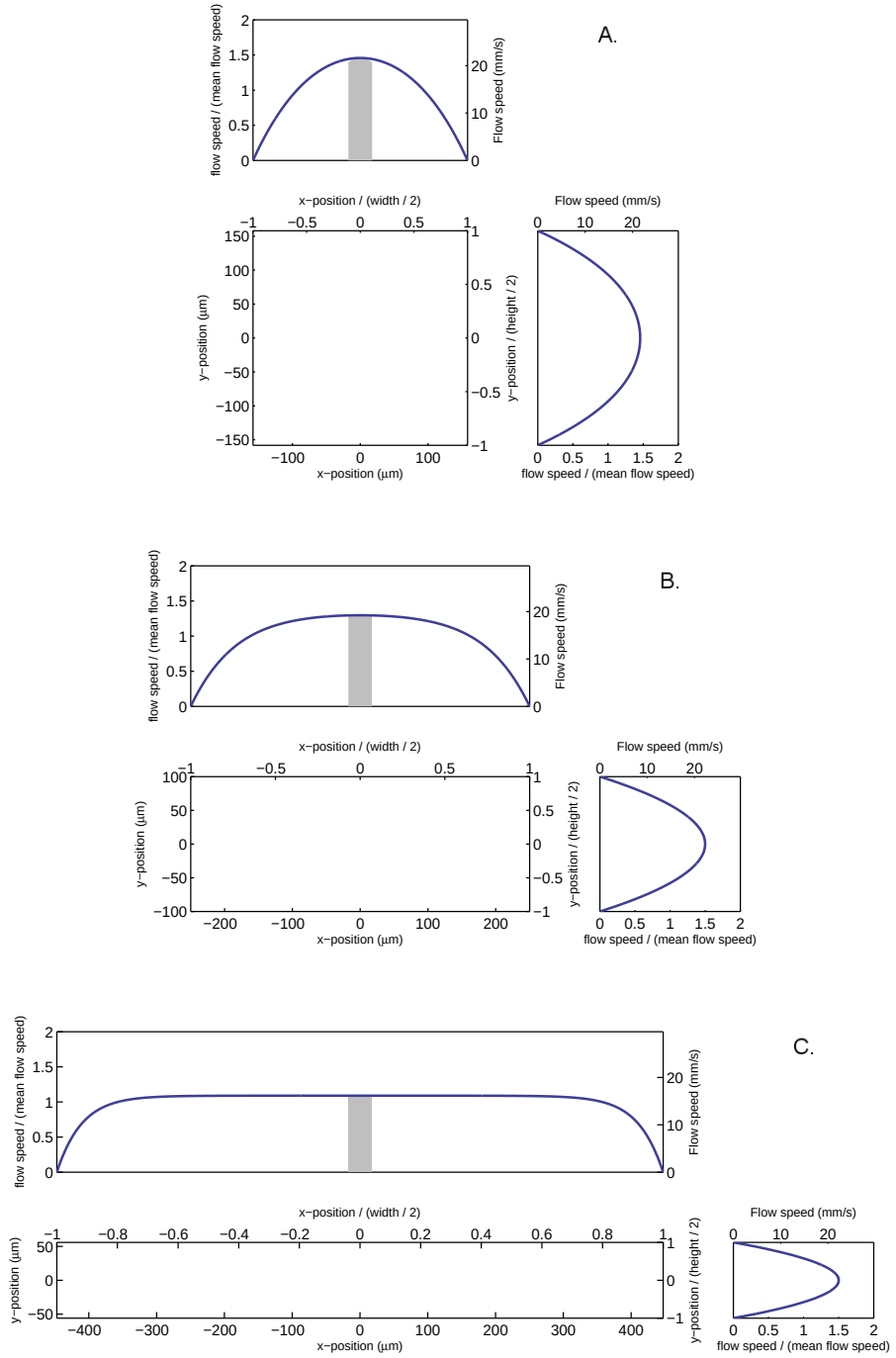

Figure 3.3: Flow speed profiles for different channel dimensions for volume flow rate $60\,\mu\mathrm{L\,min^{-1}}$. Indicated in gray the part of the channel projected onto the camera of width $\Delta x = 70\,\mu\mathrm{m}$, also used in the numerical average (see text). A. Square channel: ratio width:height 1:1. B. Our flow channel: ratio width:height 2.5:1. C. Flattened flow channel: ratio width:height 8:1.

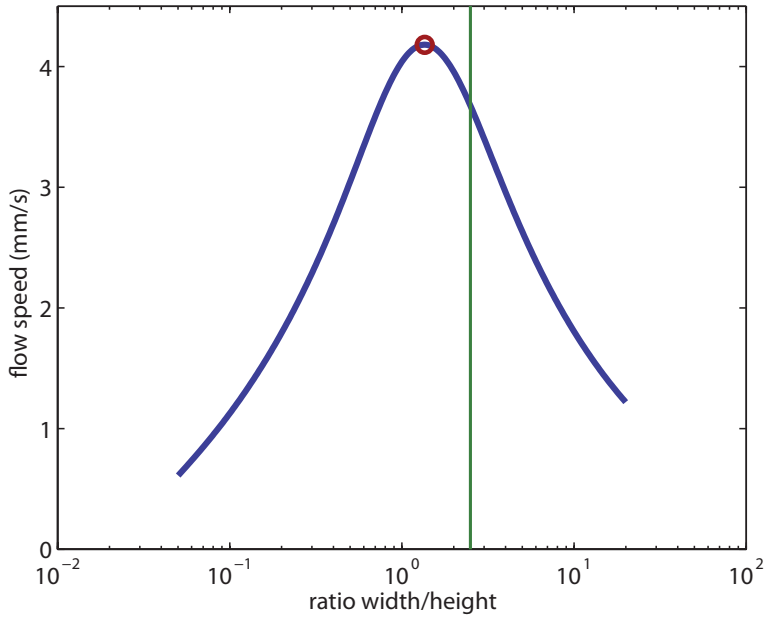

Figure 3.4: Average flow speed over central $70\,\mu$m in x-direction versus channel ratio $r = \text{width/height}$ at $y = 10\,\mu$m. The maximum at 1.3:1 is indicated with a circle. The ratio 2.5:1 is indicated with a line.

4 Results

4.1 Dengue hemifusion

One lab [Zaitseva et al., 2010] has reported a bulk fusion assay describing the rate and extent of membrane fusion by the dengue virus. Their results indicated that the presence of an anionic lipid is crucial for hemifusion to take place. However, it had not been possible to reproduce these results in the bulk so far. This irreproducibility may have to do with the relative mix of immature and mature virions, in which case the bulk assay might not be sensitive enough to detect the fusion that does take place from the mature particles. In this case it would be ideal to utilize single-particle studies and investigate whether fusion actually occurs.

Preliminary results of using dengue in the single-molecule assay found that 37 % of the viruses underwent hemifusion at room temperature and at pH 4.5. A negatively charged lipid was used (DOPG), see table 4.1, without which no hemifusion could be observed. To overcome electrostatic repulsion between the negatively charged glass surface and the anionic lipid head groups, the glass was functionalized with aminopropylsilane, forming a positively charged surface that led to good bilayer formation, as confirmed by fluorescence recovery after photobleaching (FRAP) measurements.

The sample shows a single-exponential decay with hemifsuion rate constant of $0.067 \pm 0.005\,\mathrm{s}^{-1}$ or a characteristic fusion time of $1/A = 15 \pm 2\,\mathrm{s}$. The potentially existing population at $t = 50\,\mathrm{s}$ should be confirmed with more experiments.

4.2 Chikungunya hemifusion at $37\,^{\circ}\mathrm{C}$

The first chikungunya single-particle hemifusion results in bulk (Van Oijen lab, unpublished) showed hemifusion times in the order of seconds at room temperature. To compare the single-particle results with bulk fusion assays already undertaken at by

Lipid	Fraction
DOPC	0.5
DOPG	0.5
Biotin-PE	$8 \cdot 10^{-5}$

Table 4.1: Lipid composition used for dengue experiment.

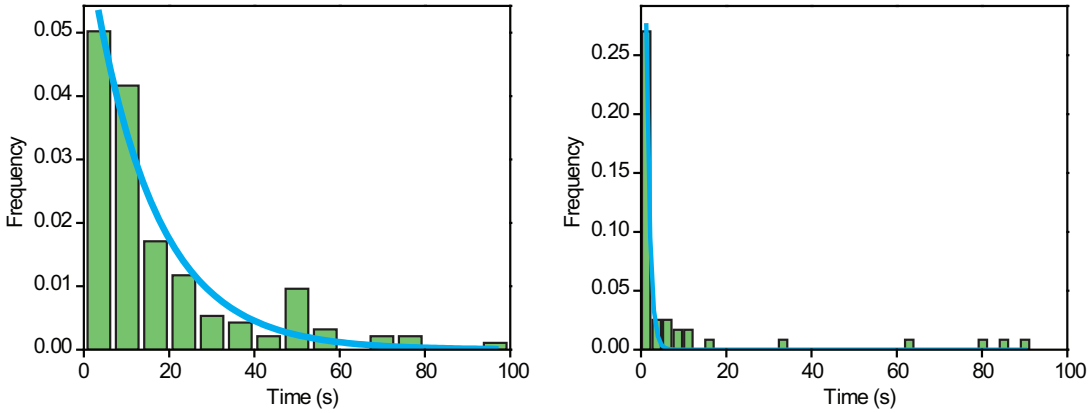

(a) (b)

Figure 4.1: (a) Denv virion hemifusion time distribution, pH 4.5, room temperature. The solid line is a fit of a single-exponential decay with rate constant $0.067 \pm 0.005\,\mathrm{s}^{-1}$. Result obtained by M. Ruiz Silva in collaboration (unpublished). (b) Chikv virion hemifusion time distribution, pH 4.5, 37 °C. The solid line is a fit of a single-exponential decay with rate constant $1.18 \pm 0.06\,\mathrm{s}^{-1}$.

Lipid	Fraction
DOPC	0.22
DOPE	0.22
Sphingomyelin	0.22
Cholesterol	0.33
B-PE	$8 \cdot 10^{-5}$

Table 4.2: Lipid composition used for the chikungunya experiments.

collaborators at UMCG, the single-particle assay needs to be performed at 37 °C (see subsection 4.2.1).

In the original experimental design the inflow of pH buffer at room temperature would cool down the heated flow cell too much, noticeable and quantifiable by focal drift. A very low yield experiment using a makeshift solution of pre-heating the inrushing pH buffer, confirmed chikunguya's short hemifusion timescales. The decay rate was found to be $1.18 \pm 0.06\,\mathrm{s}^{-1}$, see figure 4.1b, yielding a characteristic hemifsusion time of $0.9 \pm 0.2\,\mathrm{s}$ at pH 4.5. The lipid composition used is in table 4.2. This implies that short acquisition times must be used, thus increasing noise levels. The pH drop time should be controllable and short as well.

Additional experiments showed that the pH drop was in fact too slow to be able to reliably extract the chikungunya hemifusion rates. Figure 4.2 shows results obtained at several pH points, showing that for pH $\lesssim 5.5$ the pH drop, taking about 5 s, convolutes the chikungunya hemifusion events because of the fast hemifusion dynamics as found

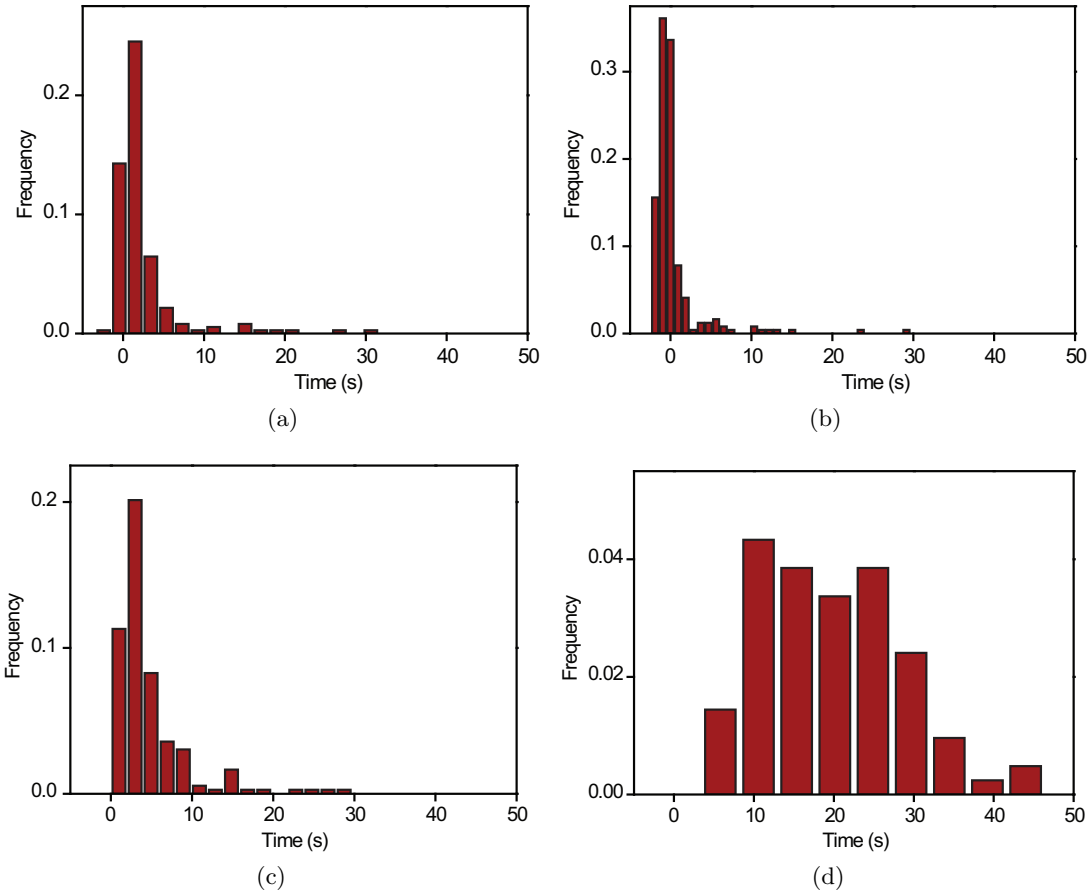

Figure 4.2: Chikv hemifusion time distribiution, 37 °C. (a) pH 4.5 and (b) pH 5.0; note the negative hemifusion times and rise-and-decay distributions due to the pH drops of ~ 5 s. (c) pH 5.5 (d) pH 6.0

earlier. The newest design addressing this shortcoming is almost functional as explained in the next subsection.

4.2.1 New flow cell design

The initial idea of pre-heating the inflowing pH buffer so that it would reach the flow channel at elevated temperature was unstable and had unwieldy handling requirements.

A new flow cell was designed, containing a long serpentine to pre-heat the low pH buffer before flowing it into the portion of the channel visualized during fusion recordings (figure 4.3). The serpentine being very proximal to the channel makes pH drops on the order of a second possible. To prevent premature mixing of the low pH buffer, three inlets are used in a specific order, see figure 4.4.

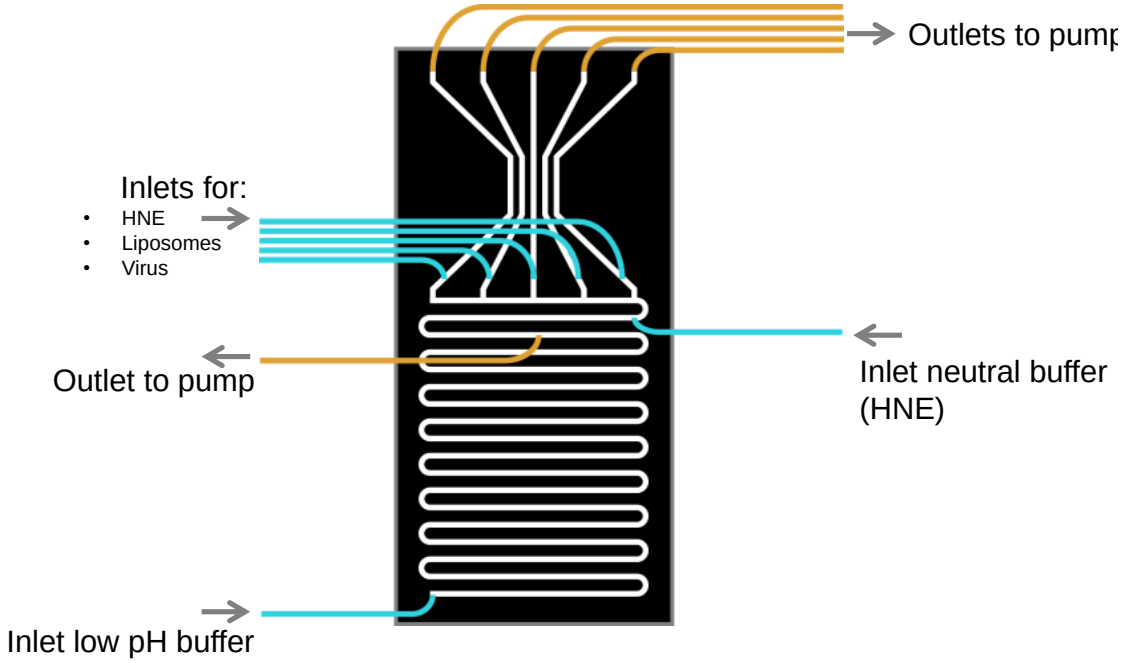

Figure 4.3: New flow cell inlets and outlets.

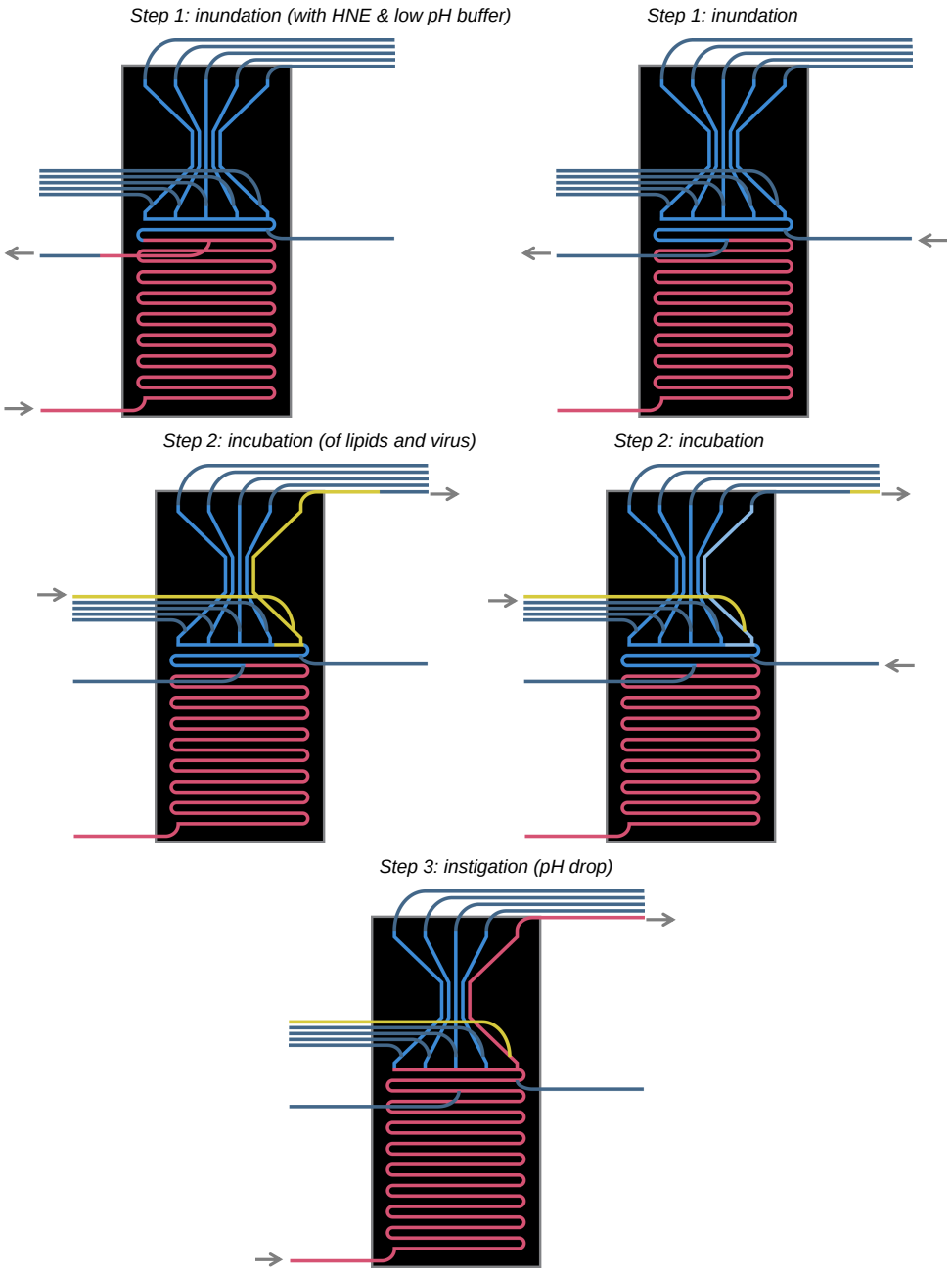

Figure 4.4: New flow cell experimental steps. pH buffer in red, HNE buffer in blue, virus and lipid incubation in yellow.

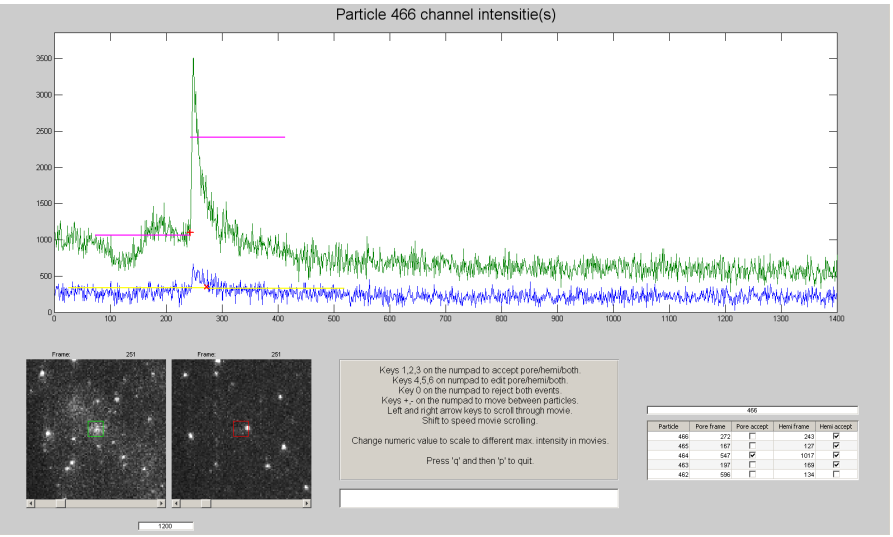

Figure 4.5: New viral fusion analasys GUI. The top graph shows the particle intensities of the two color channels. In the bottom left are the regions of interest around the particle in each of the color channels.

4.3 Viral fusion analysis

As described in section 2.3, the particle selection was done by hand by selecting all the particle intensity graphs on printed paper. In case of doubt about an intensity trajectory showing an event or not, inefficient switching between computer programs and windows had to be done. A new GUI was developed to facilitate easier scrutiny of single-particle intensity trajectories, see figure 4.5. Using shortcuts, one can now quickly sort through the trajectories. In the same window. one can have a look at the movie itself in case the intensity graph is unclear. The whole package is easily customizable for single-color or multiple-color channels.

A stand-alone package to do automated viral fusion analysis is currently in progress working together with J. Otterstrom.

5 Conclusion

The flow cell geometry that gives the fastest flow speed for a given volume flow rate at the lipid bilayer surface was determined numerically to be $r = 1.3$. The current design is close to optimal, and due to the pH diffusion playing a large role in the acidification time a re-design is not warranted. The force acting on the virus particles for volume flow rate $300\,\mu\mathrm{L}\cdot\mathrm{min}^{-1}$ was calculated to be 50 pN.

Dengue hemifusion was observed. The sample, although yet limited in size, shows a rate constant of $0.067 \pm 0.005\,\mathrm{s}^{-1}$ or a characteristic fusion time of $15 \pm 2\,\mathrm{s}$ at pH 4.5. More statistics are needed to see if there are in fact multiple populations present, as may be suggested by a peak at $t = 50\,\mathrm{s}$. Chikungunya hemifusion was observed at high temperature with a rate constant of $1.18 \pm 0.06\,\mathrm{s}^{-1}$, yielding a characteristic hemifusion time of $0.9 \pm 0.2\,\mathrm{s}$ at pH 4.5. The challenge to ensure an acidification time shorter than this whilst maintaining a constant high temperature was addressed with a new flow channel design. Furthermore, to facilitate future data analysis the foundation a an automatic analysis software package was laid in a collaboration.

The single-particle study of chikungunya as begun in this report is both pioneering and a promising road towards antibody screening. More research towards the lipid and pH dependency of both chikungunya and dengue fusion will help to unravel their specific fusion mechanisms and be invaluable for the development of single-particle antibody screening assays.

6 Acknowledgements

The author would like to thank Antoine for providing a place where physics and biology meet in a fantastic way, where many nationalities and very amicable group members meet, and for his competitive attitude in the Ardennes. The author found Jason's direct help, advice and also allowing the freedom to make mistakes indispensable and is very grateful for that. Sarah, Karl, Andrew and in fact all other SMB groupmembers the author would like to thank for their help and lunchbreaks. Special thanks go to Mareike Richter, Mariana Ruiz Silva and their professor Jolanda Smit for their collaboration.

Bibliography

N. Agmon. The grotthuss mechanism. *Chemical Physics Letters*, 244(5):456–462, 1995. URL http://www.sciencedirect.com/science/article/pii/000926149500905J.

L. P. Faucheux and A. J. Libchaber. Confined brownian motion. *Physical Review E*, 49: 5158–5163, 1994. URL http://adsabs.harvard.edu/abs/1994PhRvE..49.5158F.

D. L. Floyd, J. R. Ragains, J. J. Skehel, S. C. Harrison, and A. M. van Oijen. Single-particle kinetics of influenza virus membrane fusion. *Proceedings of the National Academy of Sciences*, 105(40):15382–15387, 2008.

R. V. Gibbons and D. W. Vaughn. Dengue: an escalating problem. *BMJ: British Medical Journal*, 324(7353):1563, 2002.

P. Goldreich, S. Mahajan, and S. Phinney. Order-of-magnitude physics: Understanding the world with dimensional analysis, educated guesswork, and white lies, 1999.

M. Kielian and F. A. Rey. Virus membrane-fusion proteins: more than one way to make a hairpin. *Nature Reviews Microbiology*, 4(1):67–76, 2006. URL http://www.nature.com/nrmicro/journal/v4/n1/abs/nrmicro1326.html.

C. S.-S. Martín, C. Y. Liu, and M. Kielian. Dealing with low ph: entry and exit of alphaviruses and flaviviruses. *Trends in Microbiology*, 17(11):514–521, 2009. URL http://www.sciencedirect.com/science/article/pii/S0966842X09001693.

G. Pialoux, B.-A. Gaüzère, S. Jauréguiberry, and M. Strobel. Chikungunya, an epidemic arbovirosis. *The Lancet infectious diseases*, 7(5):319–327, 2007. URL http://www.sciencedirect.com/science/article/pii/S147330990770107X.

E. M. Purcell. Life at low reynolds number. In *AIP Conference Proceedings*, volume 28, page 49, 1976. URL http://pdfserv.aip.org/APCPCS/vol_28/iss_1/49_1.pdf.

J. Schön and M. Weidner. Gauged n= 4 supergravities. *Journal of High Energy Physics*, 2006(05):034, 2006. URL http://iopscience.iop.org/1126-6708/2006/05/034.

O. Schwartz and M. L. Albert. Biology and pathogenesis of chikungunya virus. *Nature Reviews Microbiology*, 8(7):491–500, 2010. URL http://www.nature.com/nrmicro/journal/v8/n7/abs/nrmicro2368.html.

R. Sjöback, J. Nygren, and M. Kubista. Absorption and fluorescence properties of fluorescein. *Spectrochimica Acta Part A: Molecular and Biomolecular Spectroscopy*, 51(6):L7 – L21, 1995. ISSN 1386-1425. doi: 10.1016/0584-8539(95)01421-P. URL http://www.sciencedirect.com/science/article/pii/058485399501421P.

T. M. Squires and S. R. Quake. Microfluidics: Fluid physics at the nanoliter scale. *Reviews of modern physics*, 77(3):977, 2005. URL http://rmp.aps.org/abstract/RMP/v77/i3/p977_1.

H. A. Stone. Introduction to fluid dynamics for microfluidic flows. In *CMOS Biotechnology*, pages 5–30. Springer, 2007. URL http://link.springer.com/content/pdf/10.1007/978-0-387-68913-5_2.pdf.

E. Zaitseva, S.-T. Yang, K. Melikov, S. Pourmal, and L. V. Chernomordik. Dengue virus ensures its fusion in late endosomes using compartment-specific lipids. *PLoS pathogens*, 6(10):e1001131, 2010. URL http://dx.plos.org/10.1371/journal.ppat.1001131.